PNAS RESEARCH ARTICLE | BIOCHEMISTRY

Dynamic investigation of hypoxia-induced L-lactylation

Jinjun Gao[a,1], Ruilong Liu[a], Kevin Huang[b], Ziyuan Li[c], Xinlei Sheng[a], Kasturi Chakraborty[a], Chang Han[a], Di Zhang[d,e], Lev Becker[a], and Yingming Zhao[a,2]

Affiliations are included on p. 10.

Edited by Melanie Cobb, The University of Texas Southwestern Medical Center, Dallas, TX; received March 15, 2024; accepted December 6, 2024

The recently identified histone modification lysine lactylation can be stimulated by L-lactate and glycolysis. Although the chemical group added upon lysine lactylation was originally proposed to be the L-enantiomer of lactate ($K_{L\text{-}la}$), two isomeric modifications, lysine D-lactylation ($K_{D\text{-}la}$) and N-ε-(carboxyethyl) lysine (K_{ce}), also exist in cells, with their precursors being metabolites of glycolysis. The dynamic regulation and differences among these three modifications in response to hypoxia remain poorly understood. In this study, we demonstrate that intracellular $K_{L\text{-}la}$, but not $K_{D\text{-}la}$ or K_{ce}, is up-regulated in response to hypoxia. Depletion of glyoxalase enzymes, GLO1 and GLO2, had minimal impact on $K_{D\text{-}la}$, K_{ce}, or hypoxia-induced $K_{L\text{-}la}$. Conversely, blocking glycolytic flux to L-lactate under hypoxic conditions by knocking out lactate dehydrogenase A/B completely abolished the induction of $K_{L\text{-}la}$ but increased $K_{D\text{-}la}$ and K_{ce}. We further observed a correlation between the level of $K_{L\text{-}la}$ and hypoxia-inducible factor 1 alpha (HIF-1α) expression under hypoxic conditions and when small molecules were used to stabilize HIF-1α in the normoxia condition. Our result demonstrated that there is a strong correlation between HIF-1α and $K_{L\text{-}la}$ in lung cancer tissues and that patient samples with higher grade tend to have higher $K_{L\text{-}la}$ levels. Using a proteomics approach, we quantified 66 $K_{L\text{-}la}$ sites that were up-regulated by hypoxia and demonstrated that p300/CBP contributes to hypoxia-induced $K_{L\text{-}la}$. Collectively, our study demonstrates that $K_{L\text{-}la}$, rather than $K_{D\text{-}la}$ or K_{ce}, is the prevailing lysine lactylation in response to hypoxia. Our results therefore demonstrate a link between $K_{L\text{-}la}$ and the hypoxia-induced adaptation of tumor cells.

lactylation | posttranslational modification (PTM) | hypoxia | LC–MS/MS

L-lactate, traditionally considered a waste byproduct of metabolism, is elevated via enhanced glycolysis when oxygen is low (1, 2). In addition, enhanced glycolysis and elevated L-lactate generation are observed in most, if not all, cancer cells, a phenomenon known as the "Warburg effect" (3). Emerging lines of evidence suggest that L-lactate is associated with a wide range of cellular processes and contributes to pathophysiological changes (4), implying regulatory functions beyond its metabolic role. Our recent findings demonstrate that L-lactate serves as a precursor for histone L-lactylation, a positive histone mark localized in chromatin and associated with gene expression (5–7). Importantly, this modification operates through mechanisms that are distinct from the widely studied histone modification lysine acetylation (5). Protein lactylation has been implicated to play important roles in various biological processes and human diseases, such as neural excitation, Alzheimer's disease, and hepatocellular carcinoma (8).

Hypoxia is a prevalent feature of solid tumors that is caused by high cell proliferation rate and aberrant tumor vasculature. Hypoxia influences many aspects of tumor biology, including reprogrammed central metabolism, tumor angiogenesis, metastasis, and suppressed immune reactivity (9, 10). Hypoxia is associated with aggressive cancer phenotypes, encompassing resistance to radiotherapy and chemotherapy, and poor prognosis (11, 12). Hypoxia-inducible factor 1 alpha (HIF-1α) is a transcription factor that plays a crucial role in cellular adaptation to hypoxia (13–15). In response to hypoxia, HIF-1α is stabilized and induces expression of key metabolic enzymes such as pyruvate dehydrogenase kinase 1 (PDK1) and lactate dehydrogenase A (LDHA) (16). PDK1 negatively regulates the entry of pyruvate into the tricarboxylic acid (TCA) cycle, while LDHA converts pyruvate into L-lactate. Overexpression of these proteins contributes to elevated L-lactate levels, which is a hallmark of cancer cells.

Lysine modified by L-lactate ($K_{L\text{-}la}$), D-lactate ($K_{D\text{-}la}$), and the N-ε-carboxyethyl moiety (K_{ce}) are isomers (17). $K_{L\text{-}la}$ is known to be an enzyme-catalyzed protein posttranslational modification (PTM), for which p300 can act as a lactyltransferase (5) while HDAC1-3 are able to catalyze the delactylation reaction (18). In contrast, K_{ce} and $K_{D\text{-}la}$ are generated nonenzymatically through reaction of the lysine side chain's amine group with two glycolysis by-products, methylglyoxal

Significance

Our findings highlight the unique upregulation of the intracellular $K_{L\text{-}la}$ level in response to hypoxia, distinguishing it from the $K_{D\text{-}la}$ and K_{ce} modifications. The correlation between $K_{L\text{-}la}$ and hypoxia-inducible factor 1 alpha (HIF-1α) expression as well as cancer malignancy suggests the potential of $K_{L\text{-}la}$ as a hypoxia biomarker. Moreover, we observed that hypoxia-induced $K_{L\text{-}la}$ predominantly localizes to the nucleus, in contrast to the cytosolic localization of $K_{D\text{-}la}$ and K_{ce}. We further quantified 66 hypoxia-up-regulated $K_{L\text{-}la}$ sites and found that p300/CBP contributes to hypoxia-induced $K_{L\text{-}la}$, providing valuable insights for future functional studies of $K_{L\text{-}la}$ in hypoxia. This study expands our understanding of three lysine lactylation isomers in hypoxic conditions and sheds light on the metabolic regulation of $K_{L\text{-}la}$, underscoring its significance in cellular responses to hypoxia.

Competing interest statement: Y.Z. is a founder, board member, advisor to, and inventor on patents licensed to PTM Bio Inc. (Hangzhou, China and Chicago, IL) and Maponos Therapeutics Inc. (Chicago, IL). L.B. is a co-founder, board member, advisor to, and inventor on patents licensed to Onchilles Pharma Inc.; a co-founder, board member, and inventor on patents licensed to MacroLogic Inc.; and a co-founder and inventor on patents licensed to Maponos Therapeutics Inc. K.C. is an inventor on a patent licensed to MacroLogic Inc. The other authors declare no competing interests.

This article is a PNAS Direct Submission.

Copyright © 2025 the Author(s). Published by PNAS. This article is distributed under Creative Commons Attribution-NonCommercial-NoDerivatives License 4.0 (CC BY-NC-ND).

[1]Present address: State Key Laboratory of Chemical Oncogenomics, School of Chemical Biology and Biotechnology, Peking University Shenzhen Graduate School, Shenzhen 518055, China.

[2]To whom correspondence may be addressed. Email: Yingming.Zhao@uchicago.edu.

This article contains supporting information online at https://www.pnas.org/lookup/suppl/doi:10.1073/pnas.2404899122/-/DCSupplemental.

Published March 3, 2025.

Downloaded from https://www.pnas.org by Univ Joseph Fourier/INPG on October 9, 2026 from IP address 129.88.25.232.

(MGO) and S-D-lactoylglutathione (D-LGSH), respectively (19, 20) (Fig. 1). MGO is generated by fragmentation of dihydroxyacetone-phosphate (DHAP) and glyceraldehyde-3-phosphate (G3P), two intermediates of glycolysis (21). As a very reactive molecule that can conjugate with diverse proteins, MGO is associated with several pathologies including diabetes, aging, and neurodegenerative diseases. To mitigate the harmful effects of excess MGO, the glyoxalase system, composed of glyoxalase 1 (GLO1) and glyoxalase 2 (GLO2), converts MGO to D-LGSH and subsequently to D-lactate (21) (Fig. 1). Although MGO and D-LGSH exist at low concentrations [less than 10 μM in normal cells (22)], it is possible that, like L-lactate, MGO and D-LGSH are also induced by hypoxia via enhanced glycolysis. These considerations raise intriguing questions regarding the regulation patterns of $K_{L\text{-}la}$, K_{ce}, and $K_{D\text{-}la}$ by hypoxia.

In this study, we report that L-lactate, but not MGO or D-lactate, was up-regulated by hypoxia in cancer cells. Using modification-specific antibodies, we found that $K_{L\text{-}la}$, but not $K_{D\text{-}la}$ or K_{ce}, was induced in response to hypoxia. The LDHA/B double knockout abolished the elevation of $K_{L\text{-}la}$ under hypoxia, indicating the dependence of this modification on glycolysis enzymes and LDH. In contrast, deletion of the glyoxalase system (GLO1−/−, GLO2−/−, or GLO1/2−/−) did not alter hypoxia-regulated $K_{L\text{-}la}$, suggesting that regulation of $K_{L\text{-}la}$ is independent of the glyoxalase system. Furthermore, we showed that hypoxia-regulated $K_{L\text{-}la}$, but not $K_{D\text{-}la}$ or K_{ce}, was dependent on HIF-1α expression. Immunofluorescence staining revealed that hypoxia-induced $K_{L\text{-}la}$ predominantly localized to the nucleus, whereas K_{ce} and $K_{D\text{-}la}$ exhibited cytosolic localization. Finally, we quantified 66 hypoxia-up-regulated $K_{L\text{-}la}$ sites on histone proteins in response to hypoxia. Collectively, our results clearly indicate that $K_{L\text{-}la}$ is both structurally and mechanistically distinguished from $K_{D\text{-}la}$ and K_{ce}, emphasizing $K_{L\text{-}la}$ as the sole hypoxia-responsive pathway among these three modifications.

Results

Hypoxia Specifically Induces $K_{L\text{-}la}$, but Not $K_{D\text{-}la}$ or K_{ce}. To investigate whether hypoxia regulates cellular $K_{L\text{-}la}$, $K_{D\text{-}la}$, or K_{ce}, we first cultured wild-type (WT) MCF-7 cells in hypoxic conditions (1% oxygen). We then measured the intracellular concentrations of three metabolites: L-lactate, D-lactate (the catabolic product of D-LGSH), and MGO (Fig. 2*A*). As expected, the intracellular L-lactate level significantly increased upon hypoxia treatment (Fig. 2*B*). In contrast, D-lactate and MGO remained unchanged in response to hypoxia (Fig. 2 *C* and *D*). In parallel, we measured the expression levels of the enzymes catalyzing production of L-lactate (LDHA) and catabolism of MGO and D-LGSH (GLO1 and GLO2, respectively). LDHA showed a substantial upregulation after 24 h of hypoxia treatment, whereas GLO1 and GLO2 remained unaltered (Fig. 2*E* and *SI Appendix*, Fig. S1 *A*–*C*).

To investigate the regulation of $K_{L\text{-}la}$, $K_{D\text{-}la}$, and K_{ce}, we developed pan anti-$K_{D\text{-}la}$ and pan anti-K_{ce} antibodies, using the same approach as the previously established pan anti-$K_{L\text{-}la}$ antibody (5). Immunoblotting assays using random peptide libraries, bovine serum albumin (BSA), and sequence-specific histone peptides verified the high specificity of the three antibodies (23). Using these modification-specific antibodies, we evaluated intracellular $K_{L\text{-}la}$, $K_{D\text{-}la}$, and K_{ce} levels upon hypoxia treatment (Fig. 2*A*). $K_{L\text{-}la}$ was up-regulated in response to hypoxia (Fig. 2*F* and *SI Appendix*, Fig. S1*D*). However, $K_{D\text{-}la}$ and K_{ce} levels remained unchanged and at background levels (Fig. 2 *G* and *H* and *SI Appendix*, Fig. S1 *E*

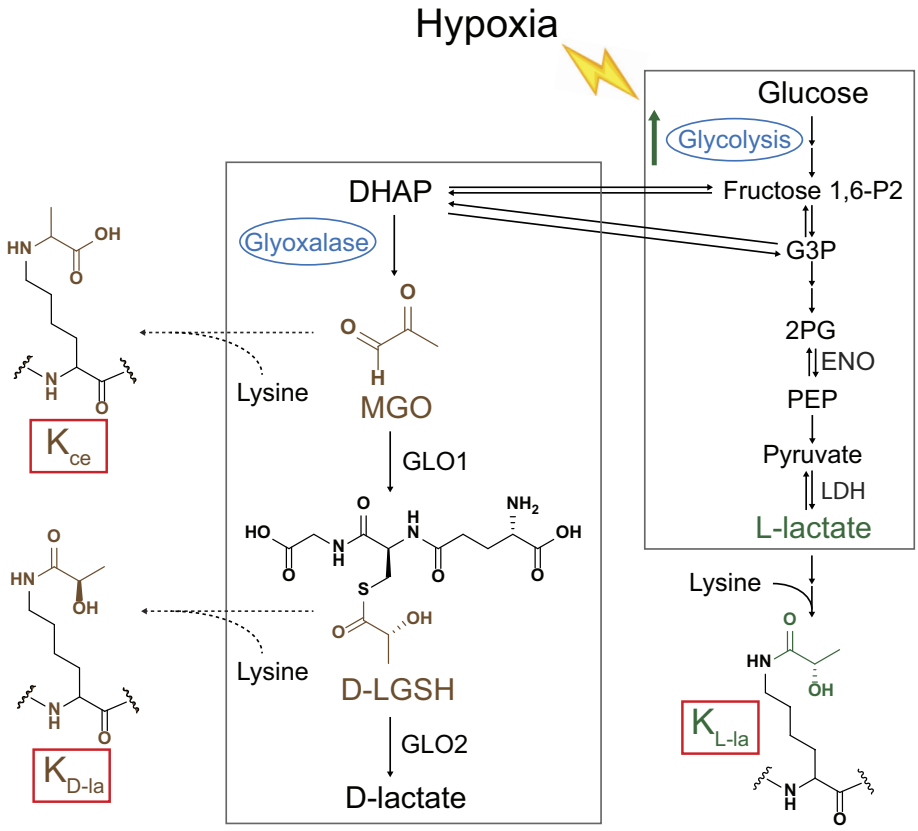


Fig. 1. Schematic representation of lysine L-lactylation ($K_{L\text{-}la}$) and its two isomers, lysine D-lactylation ($K_{D\text{-}la}$) and N-ε-(carboxyethyl) lysine (K_{ce}). K_{ce} and $K_{D\text{-}la}$ are derived from two glycolysis by-products, MGO and D-LGSH, respectively. Fructose 1,6-P2: Fructose 1,6-bisphosphate; G3P: Glyceraldehyde 3-phosphate; DHAP: Dihydroxyacetone phosphate; 2PG: 2-Phosphoglycerate; PEP: Phosphoenolpyruvate.

Downloaded from https://www.pnas.org by Univ Joseph Fourier/INPG on October 9, 2026 from IP address 129.88.25.232.

and *F*). Taken together, our results show that hypoxia induced $K_{L\text{-}la}$, but not $K_{D\text{-}la}$ or K_{ce}.

The Glyoxalase System Is Dispensable for Regulation of Hypoxia-Stimulated $K_{L\text{-}la}$. GLO1 and GLO2 play crucial roles in the metabolism of MGO and D-LGSH, respectively, which are the reactive precursors for K_{ce} and $K_{D\text{-}la}$. We therefore asked whether $K_{D\text{-}la}$ and K_{ce} levels were regulated by hypoxia in the absence of GLO1 or GLO2. To this end, we generated HEK293T cells deficient in the glyoxalase system (GLO1−/−, GLO2−/−, or GLO1/2−/−) using the CRISPR/Cas9 technology. We first compared cell proliferation rates upon hypoxia treatment between the glyoxalase-deficient and WT HEK293T cell lines to assess their adaptation to hypoxia. The same number of cells were seeded and subjected to hypoxia for 0 h to 48 h and the final cell counts were normalized to the normal (0 h) condition (*SI Appendix*, Fig. S2). The relative cell counts after hypoxia treatment were comparable across the cell lines (Fig. 3*A*). Our results suggest that deletion of the glyoxalases did not attenuate the adaptability of these cells to hypoxia. Furthermore, these gene-deficient cell lines exhibited similar expression levels of HIF-1α and LDHA compared to their WT counterpart, in which HIF-1α peaked at 12 h and LDHA gradually accumulated over 48 h (Fig. 3*B*). Consistent with the LDHA levels, the pattern of hypoxia-induced cellular $K_{L\text{-}la}$ was comparable in the WT and glyoxalase-deficient cell lines (*Upper*, Fig. 3 *C*–*F* and *SI Appendix*, Fig. S3).

Interestingly, cellular $K_{D\text{-}la}$ and K_{ce} were largely unchanged upon hypoxia treatment, regardless of the presence of the glyoxalase enzymes (*Middle* and *Lower*, Fig. 3 *C*–*F* and *SI Appendix*, Fig. S3). These observations can be explained by alternative MGO detoxification pathways in mammals, including the aldo–keto reductase (AKR) and aldehyde dehydrogenase (ALDH) enzyme families (24). Previous studies have also demonstrated that the complete loss of GLO1 does not result in elevation of MGO or MG-H1 (the major MGO-derived PTM), even under high-glucose conditions (25). Collectively, these results indicate that the regulation of neither $K_{L\text{-}la}$, $K_{D\text{-}la}$, nor K_{ce} is affected in the absence of glyoxalases in the context of hypoxia. This line of evidence also supports our finding that it is $K_{L\text{-}la}$, rather than $K_{D\text{-}la}$ or K_{ce}, that responds to hypoxia.

Deletion of Both LDHA and LDHB Suppressed $K_{L\text{-}la}$ but Stimulated $K_{D\text{-}la}$ and K_{ce} upon Hypoxia. Lactate dehydrogenases A and B (LDHA and LDHB) catalyze the reversible reaction between pyruvate and lactate. Deletion of both LDHA and LDHB has been shown to abolish the production of L-lactate (26). To further

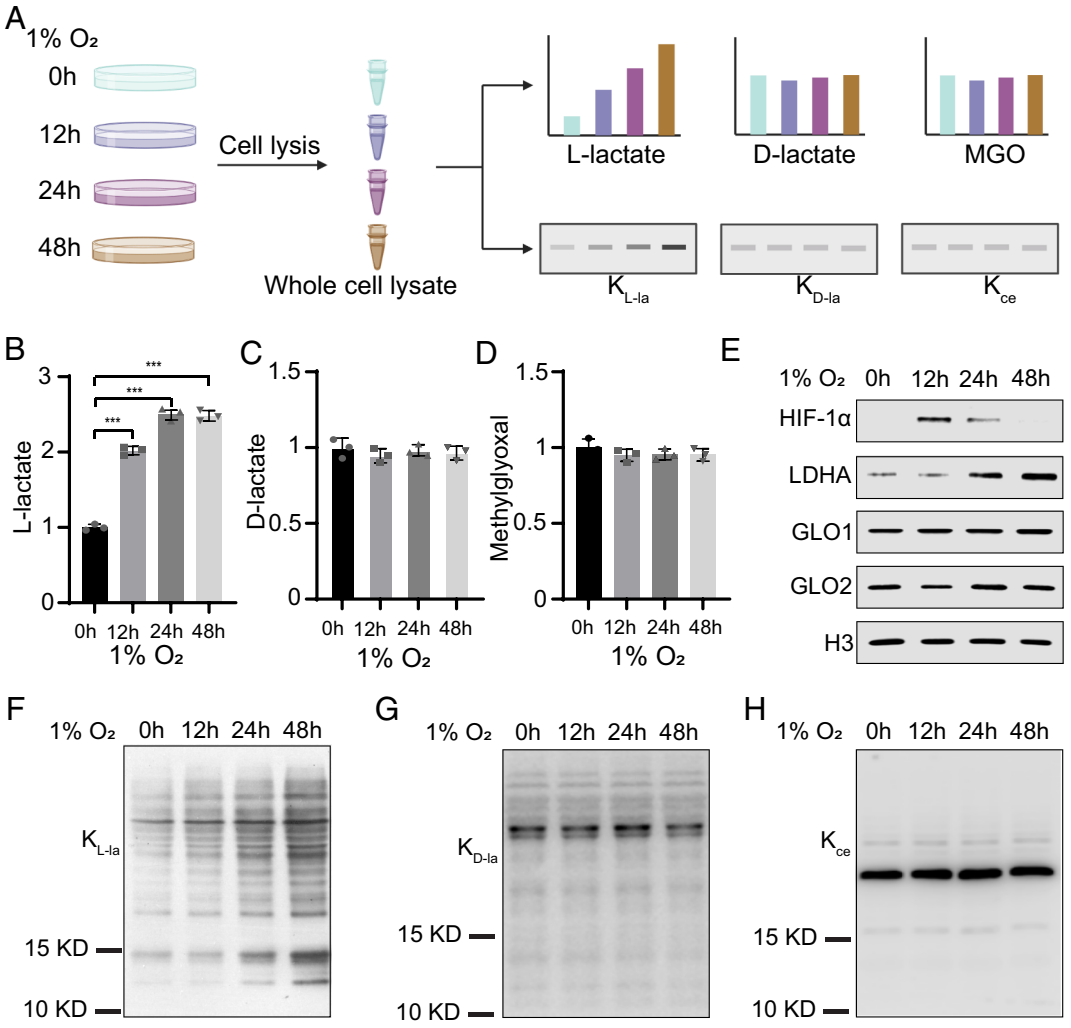


Fig. 2. Hypoxia induces $K_{L\text{-}la}$, but not $K_{D\text{-}la}$ or K_{ce}, in WT cultured cells. (*A*) Schematic representation of hypoxia workflow using WT MCF-7 cells. WT MCF-7 cells were challenged with hypoxia for indicated times (0 h, 12 h, 24 h, and 48 h), followed by measurement of intracellular concentrations of L-lactate, D-lactate, and MGO. Immunoblots were performed to detect intracellular $K_{L\text{-}la}$, $K_{D\text{-}la}$, and K_{ce} levels. (*B*–*D*) Relative intracellular levels of L-lactate, D-lactate, and MGO upon hypoxia treatment. Statistical analysis was performed by student's *t* test. *** $P < 0.001$. (*E*) Immunoblots of metabolic enzymes upon hypoxia treatment. (*F*–*H*) Immunoblots of $K_{L\text{-}la}$, $K_{D\text{-}la}$, and K_{ce} upon hypoxia treatment. The immunoblots were run in parallel to (*E*) and the same amounts of samples were loaded, so the same control was used.

Downloaded from https://www.pnas.org by Univ Joseph Fourier/INPG on October 9, 2026 from IP address 129.88.25.232.

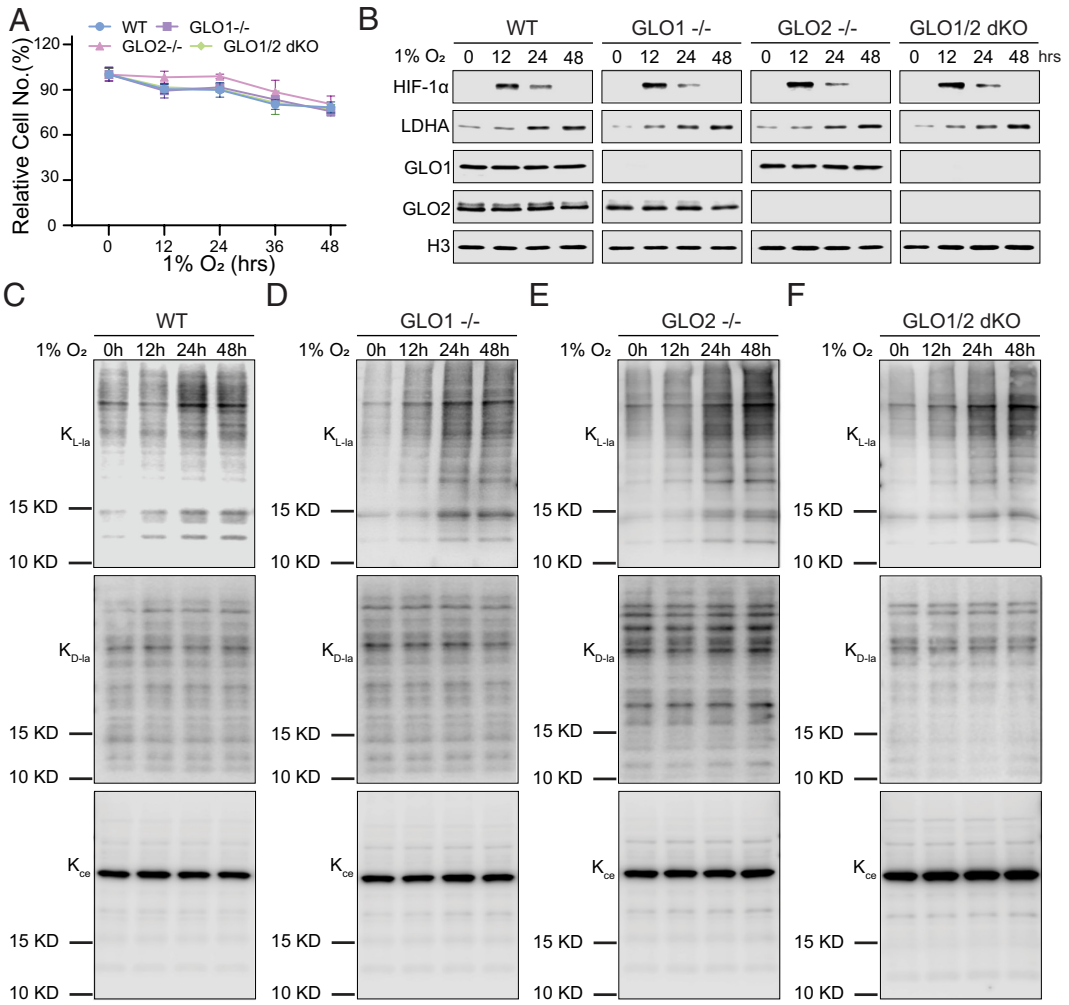


Fig. 3. Hypoxia induces $K_{L\text{-}la}$, but not $K_{D\text{-}la}$ or K_{ce}, in glyoxalase-deficient cells. (*A*) HEK293T cells deficient in the glyoxalase enzymes (GLO1−/−, GLO2−/−, or GLO1/2−/−) showed similar adaptability to hypoxia to WT cells. (*B*) Immunoblots of HIF-1α, LDHA, GLO1, and GLO2 were performed to evaluate their expression upon hypoxia treatment in WT or glyoxalase-deficient HEK293T cells. (*C*–*F*) Immunoblots of $K_{L\text{-}la}$, $K_{D\text{-}la}$, and K_{ce} in WT (*C*), GLO1−/− (*D*), GLO2−/− (*E*), and GLO1/2 dKO (*F*) HEK293T cell lines. Whole-cell lysates were collected at the indicated time points of hypoxia treatment and were used for western blot analysis. The immunoblots were run in parallel to (*B*) and the same amounts of samples were loaded, so the same control was used.

deconvolute the underlying mechanisms of $K_{L\text{-}la}$, $K_{D\text{-}la,}$ and K_{ce}, we utilized LDHA−/−, LDHB−/−, and LDHA/B−/− HepG2 cell lines which were generated as previously described (5). The proliferation rates of these cell lines under hypoxia were analyzed as described above (*SI Appendix*, Fig. S2). The single deletion of either LDHA or LDHB did not compromise adaptation to hypoxia (Fig. 4*A*). This was anticipated, given the compensatory relationship between LDHA and LDHB. In contrast, double knockout of LDHA and LDHB (LDHA/B−/−) significantly impaired the proliferation rate, indicating the crucial role of LDH in adaptation to hypoxia (Fig. 4*A*). Knocking out LDHA and LDHB did not impact the protein abundances of GLO1 and GLO2 after hypoxia treatment for 24 h (Fig. 4*B*).

We next examined how deletion of LDH affects the regulation of $K_{L\text{-}la}$, $K_{D\text{-}la,}$ and K_{ce} upon hypoxia treatment. In the single deletion cell lines LDHA−/− and LDHB−/−, we observed a slight decrease of $K_{L\text{-}la}$, while the double knockout LDHA/B−/− cell line exhibited a significant reduction of $K_{L\text{-}la}$ (Fig. 4*C* and *SI Appendix*, Fig. S4*A*). As a positive control, the induction of $K_{L\text{-}la}$ was still observed in LDHA/B−/− cells treated with 25 mM L-lactate (Fig. 4*C* and *SI Appendix*, Fig. S4*A*). This result suggests the essential yet compensatory roles of LDHA and LDHB in mediating $K_{L\text{-}la}$. On the other hand, deletion of either LDHA or LDHB individually did not lead to significant changes in $K_{D\text{-}la}$ or K_{ce} in either normoxic or hypoxic conditions (Fig. 4 *D* and *E*). However, the LDHA/B−/− cell line displayed a dramatic increase in $K_{D\text{-}la}$ and K_{ce} in hypoxia (Fig. 4 *D* and *E* and *SI Appendix*, Fig. S4 *B* and *C*). Knocking out of the two genes could redirect the glycolytic flux to the glyoxalase pathway, leading to the elevation of $K_{D\text{-}la}$ and K_{ce}. Indeed, this observation aligns with prior studies where inhibiting PGK1 (27) and GAPDH (28) led to a significant increase in cellular MGO levels.

Together, these results indicate that $K_{L\text{-}la}$, $K_{D\text{-}la}$, and K_{ce} are differentially regulated under hypoxic conditions. Moreover, these modifications, although associated with glycolytic flux, may be regulated at different steps along the glycolysis axis.

Chemical Modulation of Glycolysis and Mitochondrial Respiration Pathways Reveals Different Responses to Hypoxia of $K_{L\text{-}la}$ Relative to $K_{D\text{-}la}$ and K_{ce}. Given that deletion of LDH enzymes can abolish $K_{L\text{-}la}$ and stimulate $K_{D\text{-}la}$ and K_{ce}, we hypothesized that modulation of glycolysis and mitochondrial pathways would also differentially regulate these modifications in the context of hypoxia. To test this hypothesis, we exposed WT MCF-7 cells to various concentrations of small molecules that inhibit distinct steps of the glycolysis and mitochondrial respiration pathways (Fig. 5*A*).

Downloaded from https://www.pnas.org by Univ Joseph Fourier/INPG on October 9, 2026 from IP address 129.88.25.232.

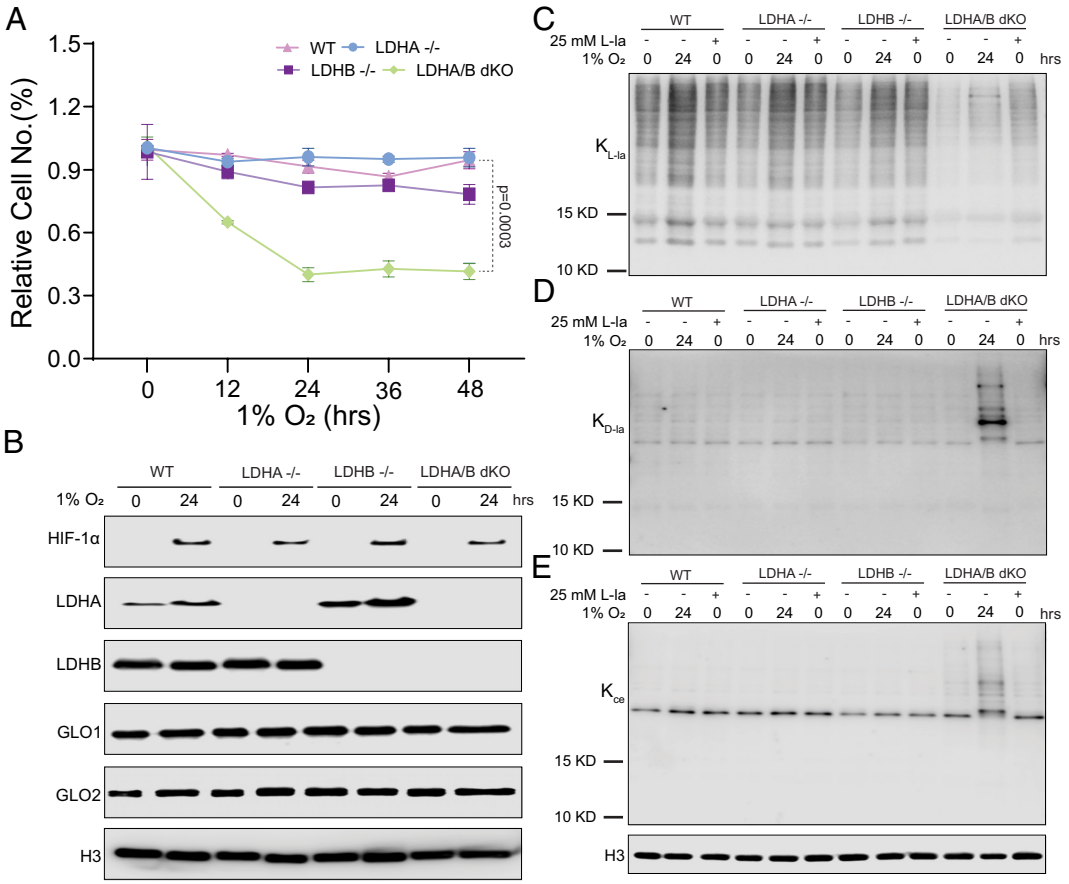


Fig. 4. Hypoxia-induced $K_{L\text{-}la}$ upregulation is abolished in LDH-deficient cells. (*A*) Single deletion of LDHA or LDHB did not compromise hypoxia adaptation compared to WT cells. Double knockout of LDHA and LDHB significantly reduced the cell proliferation rate under hypoxic conditions. Statistical analysis was performed by Student's *t* test. (*B*) Immunoblots of HIF-1α, LDHA, LDHB, GLO1, and GLO2 were performed to evaluate their expression upon hypoxia treatment in either WT or LDH-deficient HepG2 cell lines. (*C–E*) Immunoblots of $K_{L\text{-}la}$ (*C*), $K_{D\text{-}la}$ (*D*), and K_{ce} (*E*) in either WT or LDH-deficient HepG2 cells with either 24 h hypoxia or 25 mM L-lactate treatment.

Rotenone, an inhibitor of complex I of the mitochondrial electron transport chain, can switch cellular metabolism toward glycolysis (29). As expected, rotenone treatment led to an upregulation of $K_{L\text{-}la}$ in both normoxic and hypoxic conditions, without affecting $K_{D\text{-}la}$ or K_{ce} (*SI Appendix*, Fig. S5 *A–D*). Conversely, sodium dichloroacetate (DCA), an inhibitor of pyruvate dehydrogenase kinase (PDK) that can enhance mitochondrial respiration (30), strongly repressed the hypoxia-induced $K_{L\text{-}la}$ (*SI Appendix*, Fig. S5 *A* and *B*). Although DCA slightly decreased $K_{D\text{-}la}$ and K_{ce}, there was no apparent difference between normoxia and hypoxia (*SI Appendix*, Fig. S5 *A*, *C*, and *D*). A similar effect was observed upon treatment with 2-deoxy-D-glucose (2-DG), a glucose antimetabolite that inhibits glycolysis by blocking hexokinase and glucose-6-phosphate isomerase (31). Treatment with 2-DG lowered hypoxia-induced $K_{L\text{-}la}$, while $K_{D\text{-}la}$ and K_{ce} levels also slightly decreased (*SI Appendix*, Fig. S5 *A–D*). The decrease of $K_{D\text{-}la}$ and K_{ce} can be explained by reduced flux through glycolysis and the glyoxalase branch. Therefore, we speculated that inhibiting glycolytic enzymes downstream of G3P, where the glyoxalase pathway branches, would lead to accumulation of MGO and D-LGSH, thus inducing $K_{D\text{-}la}$ and K_{ce}. To test this possibility, we treated cells with POMHEX, a potent inhibitor of enolase that blocks the production of phosphoenolpyruvate (32). Indeed, POMHEX decreased $K_{L\text{-}la}$ while slightly increasing $K_{D\text{-}la}$ and K_{ce} in both normoxia and hypoxia conditions (*SI Appendix*, Fig. S5 *A–D*). Treatment of cells with koningic acid, a potent and selective GAPDH inhibitor (33), significantly decreased $K_{L\text{-}la}$ while increasing $K_{D\text{-}la}$ and K_{ce} in both normoxia and hypoxia conditions (*SI Appendix*, Fig. S5 *E–H*). Together, these data further corroborate our hypothesis that hypoxia induces $K_{L\text{-}la}$ only and that $K_{L\text{-}la}$, $K_{D\text{-}la}$, and K_{ce} are regulated by distinct mechanisms.

Modulating HIF-1α Activity Governs $K_{L\text{-}la}$ Levels. HIF-1α is the primary transcription factor that mediates cell response and adaption to hypoxic stress (13). Thus, we postulated that modulating HIF-1α activity would result in differential regulation of $K_{L\text{-}la}$, $K_{D\text{-}la}$, and K_{ce} levels. Under normoxia conditions, HIF-1α undergoes hydroxylation by HIF-specific prolyl-hydroxylases (PHDs), followed by degradation by the von Hippel–Lindau (VHL) protein, an E3 ubiquitin ligase (13). Under hypoxia conditions, PHD activity is diminished, such that the stabilized HIF-1α can activate the glycolysis pathway. We first treated MCF-7 cells with VH-298 (34), a VHL inhibitor, under normoxia conditions. As expected, VH-298 treatment led to HIF-1α stabilization, resulting in increased LDHA expression and $K_{L\text{-}la}$ levels, while $K_{D\text{-}la}$ and K_{ce} levels remained unchanged (Fig. 5*B* and *SI Appendix*, Fig. S6 *B*, *E*, and *H*).

We further examined the effects of PX-478, a potent HIF-1α inhibitor that has been shown to suppress several aggressive human tumors (35). PX-478 (10 to 40 μM) led to a dose-dependent reduction of hypoxia-induced HIF-1α levels, leading to decreased LDHA and $K_{L\text{-}la}$ levels (Fig. 5*C* and *SI Appendix*, Fig. S6*C*). Again, $K_{D\text{-}la}$ and K_{ce} levels remained unaffected (Fig. 5*C* and *SI Appendix*, Fig. S6 *F* and *I*). Consistent with this observation, inhibition of HIF-1α indirectly with R59949, a PHD agonist, yielded similar trends (*SI Appendix*, Fig. S6 *A*, *D*, *G*, and *J*). These results strongly

Downloaded from https://www.pnas.org by Univ Joseph Fourier/INPG on October 9, 2026 from IP address 129.88.25.232.

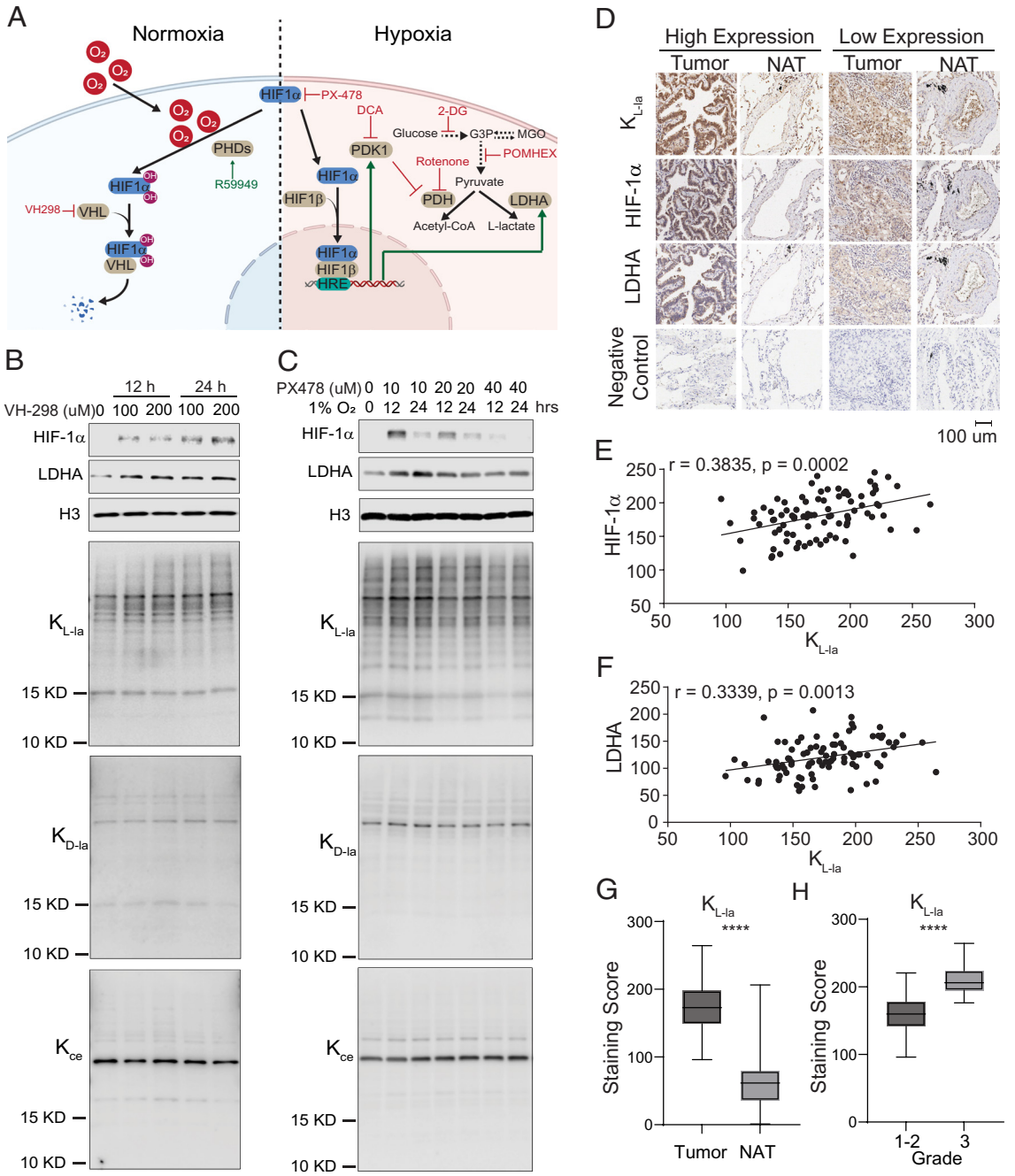


Fig. 5. $K_{L\text{-}la}$ correlates with hypoxia and cancer malignancy. (*A*) Schematic showing the HIF-1α degradation pathway under normoxia and HIF-1α-induced transcription in response to hypoxia. Molecules in red (antagonists) and green (agonists) are used to modulate the HIF-1α-mediated pathways. (*B*) Immunoblots of whole-cell lysates of MCF-7 cells in response to VHL inhibitor, which stabilizes HIF-1α in normoxic conditions. (*C*) Immunoblots of whole-cell lysates of MCF-7 cells in response to hypoxia coupled with PX478, which inhibits HIF-1α-mediated transcription in response to hypoxia. (*D*) Representative images from human lung adenocarcinoma tissue microarrays stained for $K_{L\text{-}la}$, HIF-1α, LDHA, and a negative control by omitting the primary antibody. (*E*) Pearson's correlation for all tumor samples between $K_{L\text{-}la}$ and HIF-1α staining. (*F*) Pearson's correlation for all tumor samples between $K_{L\text{-}la}$ and LDHA staining. (*G*) Distribution of staining scores for tumor and normal adjacent tissues (n = 90). (*H*) Distribution of staining scores for grade 1-2 tumor (n = 64) and grade 3 (n = 26) tumor tissues. Statistical analysis was performed by Student's *t* test. NAT: normal adjacent tissue.

support the notion that HIF-1α activity governs $K_{L\text{-}la}$, but not $K_{D\text{-}la}$ or K_{ce}.

$K_{L\text{-}la}$ Level Correlates with Hypoxia and Cancer Malignancy in Lung Adenocarcinoma. Hypoxia is associated with anticancer drug resistance and poor survival in lung adenocarcinoma (36). To investigate the association between $K_{L\text{-}la}$ and hypoxia in lung adenocarcinoma, we performed immunohistochemistry staining of $K_{L\text{-}la}$ in patient samples, consisting of 90 pairs of tumor and normal adjacent tissues (NATs). Immunostaining of two hypoxia markers, HIF-1α and LDHA, indicate hypoxia levels. $K_{L\text{-}la}$ is positively associated with both HIF-1α and LDHA in the tumor tissues (Fig. 5 *D–F* and *SI Appendix*, Fig. S7), suggesting the positive correlation between $K_{L\text{-}la}$ and hypoxia. Furthermore, a significant upregulation of $K_{L\text{-}la}$ was observed in tumor samples compared to NATs (Fig. 5*G*). Notably, $K_{L\text{-}la}$ levels were significantly higher in grade 3 tumors compared to grade 1 to 2 tumors (Fig. 5*H*). These findings collectively suggest the close association among elevated $K_{L\text{-}la}$, hypoxia, and tumor malignancy in lung adenocarcinoma.

Downloaded from https://www.pnas.org by Univ Joseph Fourier/INPG on October 9, 2026 from IP address 129.88.25.232.

Subcellular Localization of Hypoxia-Induced $K_{L\text{-}la}$ Differs from $K_{D\text{-}la}$ and K_{ce}. Subcellular localization is crucial for understanding the dynamic roles of PTMs within cellular systems. $K_{L\text{-}la}$ is an enzymatic modification that is present on both histones and proteins within other organelles (5, 37). To examine subcellular localization of hypoxia-induced $K_{L\text{-}la}$, we first conducted immunofluorescence staining experiments for $K_{L\text{-}la}$, $K_{D\text{-}la}$, and K_{ce} under hypoxic and normoxic conditions in WT cells. Consistent with our western blot findings, only $K_{L\text{-}la}$ exhibited induction by hypoxia, while $K_{D\text{-}la}$ and K_{ce} remained unchanged. Notably, hypoxia-induced $K_{L\text{-}la}$ primarily localized to the nucleus (*SI Appendix*, Fig. S8*A*). In previous studies, high levels of MGO increased K_{ce} and $K_{D\text{-}la}$ in GLO1−/− and GLO2−/− cells, respectively (19, 20). To induce and examine the subcellular localization of K_{ce} and $K_{D\text{-}la}$, we treated GLO1−/− and GLO2−/− cells with either DMSO or 500 μM MGO. As expected, only K_{ce} was induced by MGO in GLO1−/− cells (*SI Appendix*, Fig. S8*B*), while only $K_{D\text{-}la}$ exhibited induction in GLO2−/− cells upon MGO treatment (*SI Appendix*, Fig. S8*C*). Immunofluorescence staining clearly demonstrated that both $K_{D\text{-}la}$ and K_{ce} primarily localized to the cytosol (*SI Appendix*, Fig. S8 *B* and *C*), distinguishing them from the nucleus-localized hypoxia-induced $K_{L\text{-}la}$. These findings provide further support for the conclusion that hypoxia selectively induces $K_{L\text{-}la}$, which primarily is located in the nucleus.

Mapping Hypoxia-Induced Histone $K_{L\text{-}la}$ Sites. To investigate hypoxia-regulated histone $K_{L\text{-}la}$ in a site-specific manner, we conducted a proteomic analysis using a combination of stable isotope labeling by amino acids in cell culture (SILAC)–based quantification (38), affinity enrichment, and HPLC/mass spectrometry (Fig. 6*A*). Histones were extracted from MCF-7 cells cultured in "light"- or "heavy" SILAC media, where the heavy cells

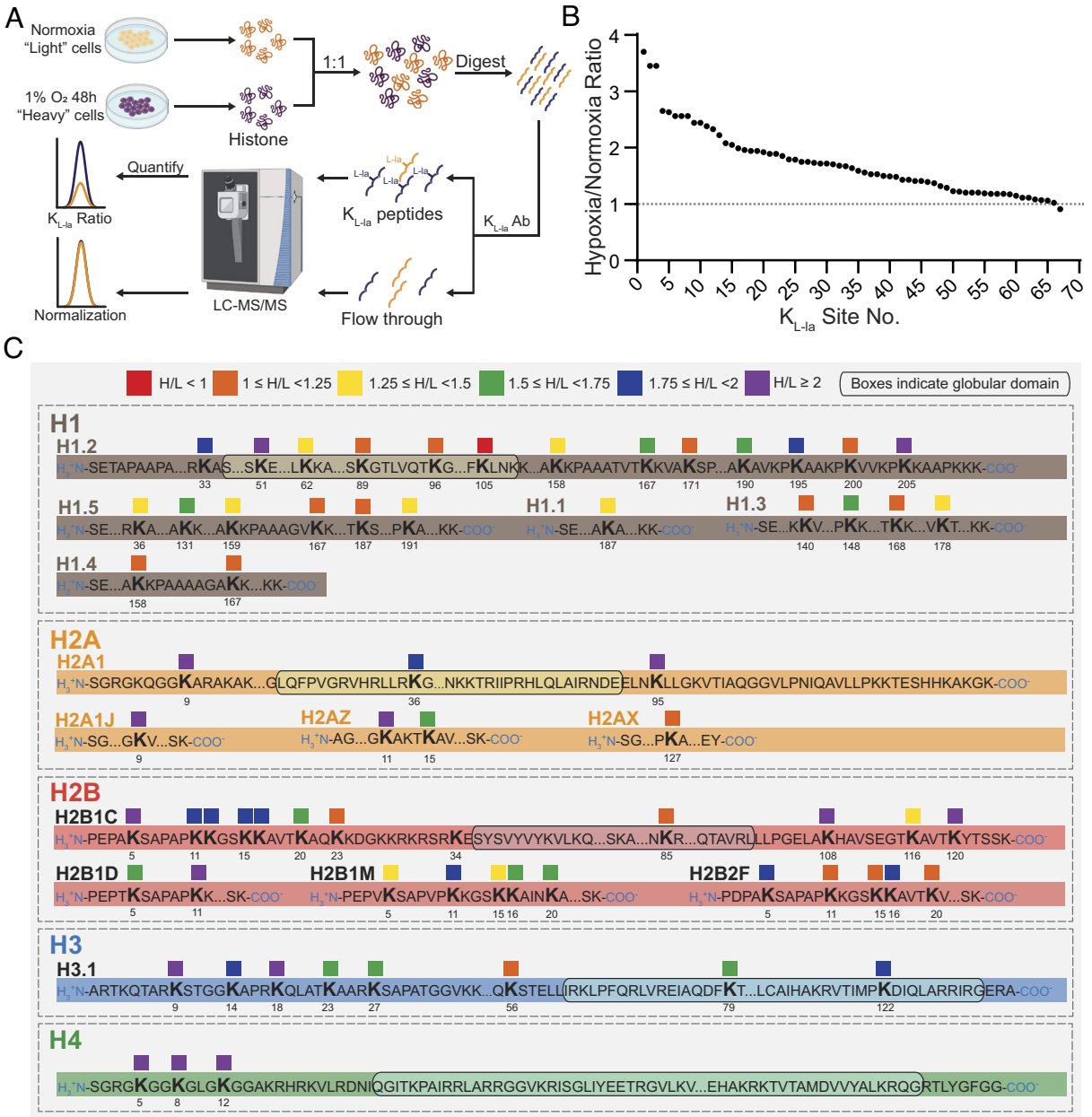


Fig. 6. The landscape of hypoxia-regulated histone $K_{L\text{-}la}$ sites. (*A*) Schematic workflow for identifying and quantifying histone $K_{L\text{-}la}$ in response to hypoxia. (*B*) Distribution of hypoxia/normoxia ratios for the quantified histone $K_{L\text{-}la}$ sites. A dashed line is drawn to indicate the ratio of 1 (unchanged). (*C*) Map of the quantified $K_{L\text{-}la}$ sites and their fold changes after hypoxia treatment. A total of 67 $K_{L\text{-}la}$ sites are marked on the corresponding histone proteins, with colors denoting the ratio ranges (red: H/L < 1; orange: 1 ≤ H/L < 1.25; yellow: 1.25 ≤ H/L < 1.5; green: 1.5 ≤ H/L < 1.75; dark blue: 1.75 ≤ H/L < 2; purple: H/L > 2). Homologous $K_{L\text{-}la}$ sites with different flanking sequences are shown separately. Boxed sequences indicate globular domains.

Downloaded from https://www.pnas.org by Univ Joseph Fourier/INPG on October 9, 2026 from IP address 129.88.25.232.

were exposed to hypoxia for 48 h. The light and heavy histones were mixed in a ratio of 1:1 (w/w) followed by trypsin digestion. Immunoprecipitation of $K_{L\text{-}la}$ peptides was performed using an anti-$K_{L\text{-}la}$ antibody, followed by HPLC–MS/MS analysis.

The database search identified a total of 103 $K_{L\text{-}la}$ sites from 166 peptides on histones, of which 112 peptides were quantified (*SI Appendix*, Fig. S9*A*). Heavy/light ratios (H/L) were derived to represent the fold changes of the 67 $K_{L\text{-}la}$ sites (Fig. 6*B* and *SI Appendix*, Fig. S9*B* and Table S1). Notably, only one $K_{L\text{-}la}$ site on the globular domains showed a slight downregulation in hypoxia (0.91 for H1.2K105), suggesting that the majority of histone $K_{L\text{-}la}$ sites are up-regulated by hypoxia. We manually examined MS/MS spectra and chromatography of the quantified peptides to ensure accurate peptide identification and quantification. All MS/MS spectra are presented (*SI Appendix*, Data S1), and the chromatographic curves of five representative $K_{L\text{-}la}$ peptides are shown (*SI Appendix*, Fig. S9*C*). These quantified histone $K_{L\text{-}la}$ sites allowed us to generate a hypoxia-regulated histone $K_{L\text{-}la}$ map (Fig. 6*C*). $K_{L\text{-}la}$ sites with identical flanking sequences were merged and depicted on one representative subtype for the major histone families: H1.2, H2A1, H2B1C, H3.1, and H4. It is intriguing to note that a few homologous $K_{L\text{-}la}$ sites are distinctively regulated by hypoxia, despite similar surrounding sequences. For instance, $K_{L\text{-}la}$ on K11 of H2B2F showed an 11% increase in hypoxia as compared to a 156% elevation for K11 of H2B1D. H2BK5 also demonstrated heterogeneous $K_{L\text{-}la}$ levels across subtypes upon hypoxia challenge (2.56 for H2B1C, 1.85 for H2B2F, 1.59 for H2B1D, and 1.43 for H2B1M). The heterogeneity across the homologous histone $K_{L\text{-}la}$ sites implies that distinct mechanisms may underlie the lactylation and delactylation processes for different histone subtypes in response to hypoxia.

p300/CBP Drives Hypoxia-Induced $K_{L\text{-}la}$. Our previous study suggested $K_{L\text{-}la}$ as an enzyme-catalyzed protein PTM, with p300 acting as a lactyltransferase (5). To investigate p300/CREB-binding protein (CBP)-mediated histone $K_{L\text{-}la}$, we used SILAC in combination with immunoprecipitation followed by HPLC/MS/MS to quantify histone peptides containing $K_{L\text{-}la}$. To this end, MCF-7 cells were cultured in either light or heavy SILAC media, treated with or without A485, a selective p300/CBP inhibitor (39), respectively. Our results confirmed that A485 treatment significantly inhibited $K_{L\text{-}la}$ levels in normoxia condition in all histone types (*SI Appendix*, Fig. S10*A*).

To investigate p300/CBP's role in hypoxia-induced $K_{L\text{-}la}$, the core histones were extracted from MCF-7 cells cultured in light and heavy SILAC media with DMSO, treated with or without hypoxia, respectively. We also carried out the same experiment as the above experiment but with 30 μM A485 added in both light and heavy SILAC media. To ensure a fair comparison of hypoxia-induced $K_{L\text{-}la}$ levels between A485 and DMSO treatments, cells were plated with the same cell number to ensure consistent cell confluences across conditions. Our quantitative proteomics experiments based on SILAC/immunoprecipitation/HPLC/MS/MS analysis showed that A485 inhibited hypoxia-induced $K_{L\text{-}la}$, although the inhibition was not complete (*SI Appendix*, Fig. S10*B*). To corroborate these observations, we carried out western blot analysis. We observed a dramatic reduction of $H3K18_{Ac}$ serving as a positive control for the A485 treatment (*SI Appendix*, Fig. S10*C*). The western blot results with pan-$K_{L\text{-}la}$ and $H3K18_{L\text{-}la}$, and $H4K8_{L\text{-}la}$ were consistent with those from the proteomics experiments (*SI Appendix*, Fig. S10 *C–F*). These results collectively suggest that p300/CPB contributes to hypoxia-induced $K_{L\text{-}la}$.

Hypoxia-Induced $K_{L\text{-}la}$ Is Associated with Activation of Glycolysis Genes. To investigate the possible roles of the histone $K_{L\text{-}la}$ in gene expression in response to hypoxia, we conducted chromatin immunoprecipitation sequencing (ChIP-Seq) experiments in MCF7 cells under conditions of normoxia and 24 h hypoxia (1% O_2) using an anti-$H3K18_{L\text{-}la}$ antibody. Pearson correlations revealed strong replicative consistency across different conditions (*SI Appendix*, Fig. S11*A*). Differential analysis of the ChIP-Seq data identified 19,179 peaks up-regulated and 16,846 peaks down-regulated under hypoxic conditions (*SI Appendix*, Fig. S11*B*). These differential peaks were predominantly enriched within promoter regions (±2 kb around transcriptional start sites) (*SI Appendix*, Fig. S11*C*), indicating involvement of $H3K18_{L\text{-}la}$ in hypoxia-induced gene regulation. To elucidate the biological significance of these genes, we performed KEGG analysis on the up-regulated genes with promoters marked by $H3K18_{L\text{-}la}$. This study revealed enrichment for multiple cancer-related pathways, including the HIF-1α signaling pathway and glycolysis/gluconeogenesis (*SI Appendix*, Fig. S11*D*). Subsequent mapping of genes to these pathways demonstrated a notable enrichment for glycolysis (*SI Appendix*, Fig. S11*E*), with all glycolysis enzymes significantly up-regulated by $H3K18_{L\text{-}la}$ under hypoxic conditions. Moreover, pyruvate dehydrogenase (PDH), which catalyzes pyruvate to acetyl-CoA, exhibited decreased counts in hypoxic conditions. These trends closely align with the metabolic shift observed in response to hypoxia, underscoring the role of $H3K18_{L\text{-}la}$ in this process. Furthermore, motif analysis of peaks with higher counts in hypoxia revealed preferential binding of $H3K18_{L\text{-}la}$ to motifs of bZIP transcription factors (TFs), with the second most prominent being bHLH, a family HIF-1α belongs to (*SI Appendix*, Fig. S11 *F* and *G*). Given the widespread involvement of both TF families in fine-tuning oxygen homeostasis in human cells, these findings further emphasize the significant role of $H3K18_{L\text{-}la}$ in hypoxic adaptation.

Discussion

$K_{L\text{-}la}$, $K_{D\text{-}la}$, and K_{ce} are isomers with identical element composition, derived from three glycolysis metabolites (L-lactate, D-LGSH, and MGO, respectively). There are documented differences among these three modifications. First, the in vivo concentrations of the three metabolites differ significantly. L-lactate typically exists at millimolar concentrations and can reach 10 to 30 mM in cancer cells (40), while plasma D-lactate is present at approximately 0.01 mM under normal conditions (41). MGO, a highly reactive metabolite, has a concentration of 1 to 10 μM in normal physiology (22). Aligned with precursor metabolite levels, $K_{D\text{-}la}$ and K_{ce} remain at background levels in cancer cells, consistent with our previous findings (23). Second, $K_{D\text{-}la}$ was not observed on histones, and only five K_{ce} sites have been found on histones, with these appearing only when GLO1−/− cells were exposed to 1 mM MGO (more than 100 times higher than its physiological concentration) for 6 h (20). In contrast, $K_{L\text{-}la}$ intensely modifies histones. Last, $K_{L\text{-}la}$ is an enzyme-catalyzed protein modification regulated by two groups of enzymes with opposite activities, similar to lysine acetylation. Conversely, $K_{D\text{-}la}$ and K_{ce} are generated by nonenzymatic chemical reactions between the lysine residue's amine group and glycolysis metabolites (D-LGSH and MGO, respectively). While HDAC1-3 and SIRT2 have been reported to remove lysine D-lactylation (18, 42), it is unknown whether additional de-D-lactylation enzymes exist in cells. Furthermore, no enzymes capable of removing K_{ce} have been reported to date.

Downloaded from https://www.pnas.org by Univ Joseph Fourier/INPG on October 9, 2026 from IP address 129.88.25.232.

The three modifications originate from distinct glycolysis metabolites, acting as their respective precursors (Fig. 1). $K_{L\text{-}la}$ is closely correlated with the concentration of L-lactate, which is known to be stimulated by glycolysis. These observations prompted us to ask whether $K_{D\text{-}la}$ or K_{ce} could also be induced in response to elevated glycolysis in general, and under hypoxic conditions in particular. It is imperative to investigate whether these three modifications are controlled by distinct mechanisms and respond differently under various physiological and pathological conditions.

Herein, we present six lines of evidence supporting differential regulation of the three modifications in the context of hypoxia. First, hypoxia specifically induced L-lactate, but not metabolites in the glyoxalase pathway. Second, hypoxia up-regulated $K_{L\text{-}la}$, which is positively correlated with L-lactate concentration, but not $K_{D\text{-}la}$ or K_{ce}. Third, in glyoxalase-deficient cell lines, $K_{L\text{-}la}$ was induced by hypoxia, while $K_{D\text{-}la}$ and K_{ce} remained unchanged. It is likely that MGO and D-LGSH can be eliminated by glyoxalase-independent pathways. This hypothesis is strengthened by previous work demonstrating that a complete loss of GLO1 did not result in an increase of MGO or MG-H1 (the major MGO-derived PTM) even under high glucose conditions (25).

Fourth, knockout of both LDHA and LDHB impacted all three modifications, reducing $K_{L\text{-}la}$ under both normoxic and hypoxic conditions, while increasing $K_{D\text{-}la}$ and K_{ce} specifically under hypoxia. During hypoxia, cellular metabolism is switched from mitochondrial respiration to anaerobic glycolysis. Therefore, blocking the production of L-lactate forced glycolytic flux into the glyoxalase pathway, elevating levels of K_{ce} and $K_{D\text{-}la}$, likely via increased concentrations of MGO and D-LGSH. This result was further corroborated with experiments in which several metabolic enzymes were inhibited by small molecules. Inhibition of the whole glycolysis pathway by 2-DG decreased both glycolysis and glyoxalase flux, reducing $K_{L\text{-}la}$, $K_{D\text{-}la}$, and K_{ce} levels. In contrast, inhibition of enolase or GAPDH (enzymes downstream of G3P) by POMHEX or koningic acid shifted glucose metabolism from production of L-lactate to the glyoxalase pathway, which decreased $K_{L\text{-}la}$ but increased $K_{D\text{-}la}$ and K_{ce}.

Fifth, chemical modulation of HIF-1α under either normoxic or hypoxic conditions revealed a strong correlation between HIF-1α and $K_{L\text{-}la}$, but not $K_{D\text{-}la}$ or K_{ce}. Finally, hypoxia-induced $K_{L\text{-}la}$ primarily localized to the nucleus, distinguishing it from the cytosolic localization of $K_{D\text{-}la}$ and K_{ce}. These observations collectively demonstrate the differential responses of $K_{L\text{-}la}$, $K_{D\text{-}la}$, and K_{ce} to hypoxia, with $K_{L\text{-}la}$ being the only modification regulated by hypoxia in WT cells.

We also identified and quantified hypoxia-responsive histone $K_{L\text{-}la}$ sites. Database search software detected 103 $K_{L\text{-}la}$ sites, of which 67 were quantified. Remarkably, among the detected $K_{L\text{-}la}$ sites, we found 7 histone marks that, to our knowledge, have not been described in prior studies (*SI Appendix*, Fig. S12). Of the 67 quantified $K_{L\text{-}la}$ sites, 66 were up-regulated. These $K_{L\text{-}la}$ sites displayed a wide range of changes, indicating site-specific regulatory mechanisms. We also found that p300/CPB mediates hypoxia-induced $K_{L\text{-}la}$. However, $K_{L\text{-}la}$ levels are still induced by hypoxia after inhibiting p300/CBP activity. Recent studies indicate that both MOF (43) and HBO1 (44) can catalyze histone $K_{L\text{-}la}$. Therefore, lactyltransferases other than p300/CBP may also contribute to the regulation hypoxia-induced histone lactylation. These observations collectively raise a series of intriguing questions. Are there other lysine lactyl-transferases and delactylases that regulate these $K_{L\text{-}la}$ sites? How do these $K_{L\text{-}la}$ sites regulate chromatin structure and function? Are these sites involved in the cellular adaption to hypoxia? Future investigations should seek to answer these questions.

Materials and Methods

Reagents. Pan anti-$K_{L\text{-}la}$ (PTM-1401RM), pan anti-$K_{D\text{-}la}$ (PTM-1429RM), and pan anti-K_{ce} (PTM-1701RM) antibodies were generated by PTM Bio, Inc. (Chicago, IL). Anti-histone H3 (9717S) and anti-LDHA (2012S) antibodies were purchased from Cell Signaling Technology, Inc. (Danvers, MA). Anti-LDHB (ABC927) antibodies were from Millipore Sigma (Burlington, MA). Anti-HIF-1α (NB100-105, for immunohistochemistry) was from Novus Biologicals, LLC (Littleton, CO); anti-HIF-1α (610959, for western blotting) was from BD Biosciences (Franklin Lakes, NJ). Anti-GLO1 (MA1-13029) and anti-GLO2 (PA5-30965) were from Thermo Fisher Scientific, Inc. (Waltham, MA). POMHEX (HY-131904), rotenone (HY-B1756), 2-deoxy-D-glucose (HY-13966), sodium dichloroacetate (HY-Y0445A), PX478 (HY-10231), VH-298 (HY-100947), and R59949 (HY-108355) were purchased from MedChemExpress (Monmouth Junction, NJ). Lactate colorimetric assay kit II (K627-100), D-lactate colorimetric assay kit (K667-100), and MGO assay kit (K500-100) were purchased from Biovision, Inc. (Milpitas, CA).

Cell Culture. Wild-type MCF-7, HEK293T, and HepG2 cells were obtained from the American Type Culture Collection. LDHA, LDHB, and LDHA/B knockout HepG2 cells (5) and GLO1, GLO2, and GLO1/2 knockout HEK293 cells were generated by CRISPR-Cas9-mediated gene deletion. Cells were cultured in Dulbecco's modified Eagle's medium (DMEM) supplemented with 10% FBS and 1% GlutaMAX (Thermo Fisher Scientific, Inc., Waltham, MA). For hypoxia treatment, cells were grown in a specialized humidified chamber equilibrated with 1% oxygen/94% nitrogen/5% carbon dioxide for the indicated time. For the SILAC experiment, WT MCF-7 cells were cultured in either heavy (L-Lys-$^{13}C_6$,$^{15}N_2$) or light (L-Lys-$^{12}C_6$,$^{14}N_2$) DMEM, supplemented with 10% dialyzed FBS (Thermo Fisher Scientific, Inc., Waltham, MA), for ten passages to achieve 99% labeling efficiency.

Cell Viability Measurement. Cells (1.0×10^4) were plated in 96-well plates with 100 μL of prewarmed medium per well (four technical replicates). For each cell type, five culture conditions were tested with a total culture time of 48 h; cells were challenged with hypoxia for the indicated time (0 h, 12 h, 24 h, 36 h, or 48 h). Cells were then incubated with MTS [3-(4,5-dimethylthiazol-2-yl)-5-(3-carboxymethoxyphenyl)-2-(4-sulfophenyl)-2H-tetrazolium] reagent (CellTiter 96® AQueous One Solution Cell Proliferation Assay, Promega Corp., Madison, WI) in 100 μL cultured medium at 37 °C for 2 h and the absorption at 490 nm was measured with a microplate reader (Thermo Fisher Scientific, Inc., Waltham, MA).

L-Lactate, D-Lactate, and MGO Measurement. L-lactate, D-lactate, and MGO were measured by lactate colorimetric assay kit II (K627-100), D-lactate colorimetric assay kit (K667-100), and MGO assay kit (K500-100), respectively. The kits were obtained from Biovision, Inc. The measurements followed the respective datasheets from the manufacturer. Briefly, for each condition, $1*10^6$ cells (for L-lactate measurement) or $1*10^7$ cells (for D-lactate and MGO measurement) were collected and homogenized in 100 μL of the corresponding assay buffer. After centrifugation at 12,000 × g for 5 min at 4 °C to remove insoluble materials, the supernatant was deproteinized using 10 kDa mw spin filters (1997-25, Biovision, Inc.). The resulting solution was then subjected to the respective assays.

Western Blot Analysis. For western blotting, whole-cell lysates were separated using 15% SDS-polyacrylamide gel electrophoresis and subsequently transferred to polyvinylidene fluoride membranes. The membranes were blocked with 3% bovine serum albumin (BSA) in TBST (20 mM Tris-HCl, pH 7.6, 150 mM NaCl, 0.1% Tween-20) at room temperature for 1 h. Next, the membranes were incubated with primary antibodies (prepared in 1% BSA, TBST) overnight in a cold room. Subsequently, the membranes were washed four times with TBST and incubated with secondary antibodies (prepared in 1% BSA, TBST) at room temperature for 1 h. Finally, the membranes were developed using a LI-COR Odyssey imager (LI-COR Biosciences, Lincoln, NE).

Immunofluorescence. WT MCF-7, HEK293T GLO1−/−, HEK293T GLO2−/− were plated in 8-well chambered cover glass dishes (C8-1.5H-N, CellVis, Mountain View, CA) prior to the experiment. After reaching 80 to 90% confluency, GLO1−/− and GLO2−/− cells were treated with DMSO or 500 μM MGO for 6 h. Hypoxia (1% O_2) treatment for WT MCF-7 cells was performed for 24 h after reaching 50% confluency. These cells were then fixed in acetone for 3 min followed by a 20 min permeabilization in PBST (1× PBS containing 0.2% TritonX-100). Cells were placed in blocking solution (5% NGS in PBST) for 1 h followed by an

Downloaded from https://www.pnas.org by Univ Joseph Fourier/INPG on October 9, 2026 from IP address 129.88.25.232.

overnight primary antibody incubation in 1% NGS in PBST. The following day cells were incubated in secondary antibody for 2 h at room temperature (RT). Cells were incubated in DAPI solution for 20 min at RT and then imaged. Between every step, cells were washed three times with 1× PBS. Confocal images were acquired on a Leica TCS SP5 II STED laser scanning confocal microscope (Leica Microsystems) equipped with a 40×/0.8 NA and 63×/1.4-NA oil-immersion objective. All image analysis was performed using Fiji ImageJ.

Tissue Microarray and Immunohistochemistry. Tissue microarrays (HLugA180Su12) comprising 90 cases of human lung adenocarcinoma tumor samples with matched normal adjacent tissues were purchased from Shanghai Outdo Biotech Co. Ltd. (Shanghai, China). The study was approved by the Ethics Committee of Shanghai Outdo Biotech Company with the protocol number SHYJS-CP-2206002, and the patients were first informed, and then their consent was taken. Immunohistochemistry staining was performed on the tissue microarray slides using anti-$K_{L\text{-}la}$ (PTM-1401RM, PTM Bio.), anti-HIF-1α (NB100-105, Novus Biologicals), and anti-LDHA antibodies (3582S, Cell Signaling Technology). Two negative control experiments were included: 1) the primary antibody was omitted, and all other processes remained constant; 2) $K_{L\text{-}la}$ antibody was preblocked with a $K_{L\text{-}la}$ peptide library before conducting the IHC staining. Quantitative analysis of the staining followed a previously reported method (45). Briefly, staining intensity was rated on a scale of 0 to 3: 0 for negative, 1 for weak, 2 for moderate, and 3 for strong. The corresponding cell percentage for each intensity scale was designated as X_0, X_1, X_2, and X_3, where the sum equaled 100. For each sample, the staining score was calculated using the formula: $1*X_1 + 2*X_2 + 3*X_3$, resulting in a range from 0 to 300.

ChIP-Seq. MCF7 cells were cultured in normoxia condition or treated with hypoxia (1% O2) for 24 h before collection for chromatin extraction. Each sample group comprised 4 × 10^6 cells and 6 μg of anti-H3K18L-la antibody. The two groups, each with three biological replicates, underwent sample preparation using the SimpleChIP Enzymatic Chromatin IP Kit with magnetic beads (Cell Signaling Technology, #9003). These samples were subsequently sent to Novogene (Sacramento, CA) for ChIP-Seq analysis following their standard protocol. Briefly, the DNA fragments were repaired, A-tailed for DNA library construction. The final DNA library was obtained by size selection and PCR amplification. Quantified libraries were pooled and sequenced on Illumina platforms, according to effective library concentration and data amount required. Raw data of fastq format were evaluated by FastQCv.0.11.4. Reads were mapped to the reference genome by BWA (46). Duplicates are labeled using SAMBLASTER and mapping quality value is calculated by MAPQ (47). Uniquely mapped reads were retained. MACS2 software was used for peak calling. The ChIP-Seq data have been deposited at the Gene Expression Omnibus (GEO) repository under the accession number GSE285693.

SILAC Sample Preparation. Heavy MCF-7 cells were challenged with hypoxia for 48 h, while light cells were cultured under normoxic conditions for the same duration before histone extraction. Histones from light or heavy MCF-7 cells were extracted as previously described (5). Extracted proteins were quantified with the Bradford protein assay (Bio-Rad Laboratories, Inc., Hercules, CA). Light and heavy histones were mixed at a ratio of 1:1 (weight/weight) and were then digested into peptides by trypsin (1:50, Promega Corp., Madison, WI) for 16.5 h in 100 mM ammonium bicarbonate (Sigma-Aldrich, Inc., St. Louis, MO). Digested peptides were then immunoprecipitated with a pan anti-$K_{L\text{-}la}$ antibody (PTM-1401, PTM Bio, Inc., Chicago, IL) as described previously (5). Enriched histone $K_{L\text{-}la}$ peptides were subjected to HPLC–MS/MS analysis.

HPLC–MS/MS Analysis. Enriched $K_{L\text{-}la}$ peptides were loaded onto a homemade silica column (12 cm length × 3 μm ID) packed with C18 resin (Maisch GmbH, Beim Bruckle, Germany). HPLC–MS/MS was performed on an Orbitrap Exploris™ 480 mass spectrometer (Thermo Fisher Scientific, Inc., Waltham, MA) coupled with an EASY-nLC 1000 system (Thermo Fisher Scientific, Inc., Waltham, MA). Mobile phase A was 0.1% formic acid in water, and mobile phase B was 0.1% formic acid in acetonitrile (v/v). The eluting flow rate was 0.3 μL/min. Samples were separated and eluted with a gradient of 5 to 35% mobile phase B in mobile phase A over 20 min. Under the positive-ion mode, full-scan mass spectra were acquired over the m/z range from 300 to 1,400 using the Orbitrap mass analyzer with mass resolution of 60,000. MS/MS fragmentation was performed in a data-dependent mode, in which the 15 most intense ions were selected for MS/MS analysis at a resolution of 15,000 using collision mode of HCD. Other important parameters: isolation window, 2.0 m/z units; default charge, 2+; normalized collision energy, 30%; maximum IT, auto; AGC target, standard; dynamic exclusion, exclude after 2 times within 20 s.

Data Analysis. MS/MS spectra were searched against the reverse-concatenated nonredundant FASTA human database compiled from the UniProt database by ProLuCID (7) with the CHiMA strategy (48). When searching light peptides, four variable modifications (+72.02113 Da for lysine L-lactylation, +42.01056 Da for lysine acetylation, +14.01565 Da for lysine and arginine monomethylation) were added. Maximum missed cleavage site number was 4. The precursor and fragmentation tolerances were 10 ppm and 40 ppm, respectively. For searching heavy peptides, database search parameters were similar to those used to search light peptides, except for an additional static modification for heavy lysine incorporation (+8.0142). ProLuCID search results were filtered and assembled by DTASelect 2.0 (14) with a criterion of more than 50% b/y ion coverage. The quantification of heavy/light ratios was performed by CIMAGE (49). The peptide-spectrum matches for all quantified peptides were manually verified as described (50).

Statistical Analysis. The significance of differences in the experimental data was determined using GraphPad Prism 9.5 software. All statistical details are described in the corresponding figure legends. For data presented without statistics, experiments were repeated at least three times to ensure reproducibility unless otherwise stated.

Data, Materials, and Software Availability. Proteomics data have been deposited in iProX (IPX0006076002, https://www.iprox.cn//page/subproject.html?id=IPX0006076002) (51). All other data are included in the manuscript and/or *SI Appendix*.

ACKNOWLEDGMENTS. We thank Iben Jensen University of Copenhagen for assistance with automated peptide synthesis and recording of ^{19}F NMR spectra. This work was supported by the University of Chicago, the Nancy and Leonard Florsheim Family Fund, and the NIH (grants GM135504, AR078555, and CA251677 to Y.Z.; R01DK102960 to L.B.).

Author affiliations: [a]Ben May Department for Cancer Research, The University of Chicago, Chicago, IL 60637; [b]College of Agriculture and Life Science, Cornell University, Ithaca, NY 14853; [c]Department of Chemistry, University of Wisconsin-Madison, Madison, WI 53706; [d]State Key Laboratory of Protein and Plant Gene Research, School of Life Sciences, Peking University, Beijing 100871, China; and [e]Peking-Tsinghua Center for Life Sciences, Academy for Advanced Interdisciplinary Studies, Peking University, Beijing 100871, China

Author contributions: J.G., L.B., and Y.Z. designed research; J.G., R.L., Z.L., X.S., K.C., and C.H. performed research; J.G. contributed new reagents/analytic tools; J.G., R.L., and K.C. analyzed data; and J.G., K.H., Z.L., X.S., D.Z., L.B., and Y.Z. wrote the paper.

1. J. D. Rabinowitz, S. Enerback, Lactate: The ugly duckling of energy metabolism. *Nat. Metab.* **2**, 566–571 (2020).
2. G. A. Brooks *et al.*, Lactate in contemporary biology: A phoenix risen. *J. Physiol.* **600**, 1229–1251 (2022).
3. N. N. Pavlova, J. Zhu, C. B. Thompson, The hallmarks of cancer metabolism: Still emerging. *Cell Metabol.* **34**, 355–377 (2022).
4. M. Certo, C. H. Tsai, V. Pucino, P. C. Ho, C. Mauro, Lactate modulation of immune responses in inflammatory versus tumour microenvironments. *Nat. Rev. Immunol.* **21**, 151–161 (2021).
5. D. Zhang *et al.*, Metabolic regulation of gene expression by histone lactylation. *Nature* **574**, 575–580 (2019).
6. M. V. Liberti, J. W. Locasale, Histone lactylation: A new role for glucose metabolism. *Trends Biochem. Sci.* **45**, 179–182 (2020).
7. L. T. Izzo, K. E. Wellen, Histone lactylation links metabolism and gene regulation. *Nature* **574**, 492–493 (2019).
8. H. Fan *et al.*, Lactylation: Novel epigenetic regulatory and therapeutic opportunities. *Am. J. Physiol. Endocrinol. Metab.* **324**, E330–E338 (2023).
9. G. L. Semenza, Oxygen sensing, hypoxia-inducible factors, and disease pathophysiology. *Annu. Rev. Pathol.* **9**, 47–71 (2014).
10. T. Cramer *et al.*, HIF-1alpha is essential for myeloid cell-mediated inflammation. *Cell* **112**, 645–657 (2003).
11. W. R. Wilson, M. P. Hay, Targeting hypoxia in cancer therapy. *Nat. Rev. Cancer* **11**, 393–410 (2011).
12. P. Lee, N. S. Chandel, M. C. Simon, Cellular adaptation to hypoxia through hypoxia inducible factors and beyond. *Nat. Rev. Mol. Cell Biol.* **21**, 268–283 (2020).

Downloaded from https://www.pnas.org by Univ Joseph Fourier/INPG on October 9, 2026 from IP address 129.88.25.232.

13. M. Ivan *et al.*, HIFalpha targeted for VHL-mediated destruction by proline hydroxylation: Implications for O2 sensing. *Science* **292**, 464–468 (2001).
14. N. V. Iyer *et al.*, Cellular and developmental control of O2 homeostasis by hypoxia-inducible factor 1 alpha. *Genes Dev.* **12**, 149–162 (1998).
15. B. Keith, R. S. Johnson, M. C. Simon, HIF1α and HIF2α: Sibling rivalry in hypoxic tumour growth and progression. *Nat. Rev. Cancer* **12**, 9–22 (2011).
16. M. Ivan, W. G. Kaelin Jr., The EGLN-HIF O(2)-sensing system: Multiple inputs and feedbacks. *Mol. Cell* **66**, 772–779 (2017).
17. C. Moreno-Yruela, M. Bæk, F. Monda, C. A. Olsen, Chiral posttranslational modification to lysine ε-amino groups. *Acc. Chem. Res.* **55**, 1456–1466 (2022).
18. C. Moreno-Yruela *et al.*, Class I histone deacetylases (HDAC1–3) are histone lysine delactylases. *Sci. Adv.* **8**, eabi6696 (2022).
19. D. O. Gaffney *et al.*, Non-enzymatic lysine lactoylation of glycolytic enzymes. *Cell Chem. Biol.* **27**, 206–213.e6 (2020).
20. J. J. Galligan *et al.*, Methylglyoxal-derived posttranslational arginine modifications are abundant histone marks. *Proc. Natl. Acad. Sci. U.S.A.* **115**, 9228–9233 (2018).
21. N. Rabbani, M. Xue, P. J. Thornalley, Activity, regulation, copy number and function in the glyoxalase system. *Biochem. Soc. Trans.* **42**, 419–424 (2014).
22. N. Rabbani, P. J. Thornalley, Measurement of methylglyoxal by stable isotopic dilution analysis LC-MS/MS with corroborative prediction in physiological samples. *Nat. Protocols* **9**, 1969–1979 (2014).
23. D. Zhang *et al.*, Lysine L-lactylation is the dominant lactylation isomer induced by glycolysis. *Nat. Chem. Biol.* **21**, 91–99 (2025).
24. D. L. Vander Jagt, L. A. Hunsaker, Methylglyoxal metabolism and diabetic complications: Roles of aldose reductase, glyoxalase-I, betaine aldehyde dehydrogenase and 2-oxoaldehyde dehydrogenase. *Chem. Biol. Interact.* **143-144**, 341–351 (2003).
25. J. Morgenstern *et al.*, Loss of glyoxalase 1 induces compensatory mechanism to achieve dicarbonyl detoxification in mammalian Schwann cells. *J. Biol. Chem.* **292**, 3224–3238 (2017).
26. M. Zdralevic *et al.*, Double genetic disruption of lactate dehydrogenases A and B is required to ablate the "Warburg effect" restricting tumor growth to oxidative metabolism. *J. Biol. Chem.* **293**, 15947–15961 (2018).
27. M. J. Bollong *et al.*, A metabolite-derived protein modification integrates glycolysis with KEAP1-NRF2 signalling. *Nature* **562**, 600–604 (2018).
28. P. J. Beisswenger, S. K. Howell, K. Smith, B. S. Szwergold, Glyceraldehyde-3-phosphate dehydrogenase activity as an independent modifier of methylglyoxal levels in diabetes. *Biochim. Biophys. Acta* **1637**, 98–106 (2003).
29. N. Li *et al.*, Mitochondrial complex I inhibitor rotenone induces apoptosis through enhancing mitochondrial reactive oxygen species production. *J. Biol. Chem.* **278**, 8516–8525 (2003).
30. S. Whitehouse, R. H. Cooper, P. J. Randle, Mechanism of activation of pyruvate dehydrogenase by dichloroacetate and other halogenated carboxylic acids. *Biochem. J.* **141**, 761–774 (1974).
31. D. Zhong *et al.*, The glycolytic inhibitor 2-deoxyglucose activates multiple prosurvival pathways through IGF1R. *J. Biol. Chem.* **284**, 23225–23233 (2009).
32. Y. H. Lin *et al.*, An enolase inhibitor for the targeted treatment of ENO1-deleted cancers. *Nat. Metab.* **2**, 1413–1426 (2020).
33. M. Kato, K. Sakai, A. Endo, Koningic acid (heptelidic acid) inhibition of glyceraldehyde-3-phosphate dehydrogenases from various sources. *Biochim. Biophys. Acta* **1120**, 113–116 (1992).
34. J. Frost, S. Rocha, A. Ciulli, Von Hippel–Lindau (VHL) small-molecule inhibitor binding increases stability and intracellular levels of VHL protein. *J. Biol. Chem.* **297**, 100910 (2021).
35. S. Welsh, R. Williams, L. Kirkpatrick, G. Paine-Murrieta, G. Powis, Antitumor activity and pharmacodynamic properties of PX-478, an inhibitor of hypoxia-inducible factor-1alpha. *Mol. Cancer Ther.* **3**, 233–244 (2004).
36. A. Salem *et al.*, Targeting hypoxia to improve non-small cell lung cancer outcome. *J. Natl. Cancer Inst.* **110**, 14–30 (2018).
37. M. Fan *et al.*, Lactate promotes endothelial-to-mesenchymal transition via Snail1 lactylation after myocardial infarction. *Sci. Adv.* **9**, eadc9465 (2023).
38. S. E. Ong *et al.*, Stable isotope labeling by amino acids in cell culture, SILAC, as a simple and accurate approach to expression proteomics. *Mol. Cell Proteomics* **1**, 376–386 (2002).
39. L. M. Lasko *et al.*, Discovery of a selective catalytic p300/CBP inhibitor that targets lineage-specific tumours. *Nature* **550**, 128–132 (2017).
40. M. Adeva-Andany *et al.*, Comprehensive review on lactate metabolism in human health. *Mitochondrion* **17**, 76–100 (2014).
41. M. D. Levitt, D. G. Levitt, Quantitative evaluation of D-lactate pathophysiology: New insights into the mechanisms involved and the many areas in need of further investigation. *Clin. Exp. Gastroenterol.* **13**, 321–337 (2020).
42. E. Q. Jennings *et al.*, Sirtuin 2 regulates protein lactoyllys modifications. *Chembiochem* **22**, 2102–2106 (2021).
43. B. Xie *et al.*, KAT8-catalyzed lactylation promotes eEF1A2-mediated protein synthesis and colorectal carcinogenesis. *Proc. Natl. Acad. Sci. U.S.A.* **121**, e2314128121 (2024).
44. Z. Niu *et al.*, HBO1 catalyzes lysine lactylation and mediates histone H3K9la to regulate gene transcription. *Nat. Commun.* **15**, 3561 (2024).
45. X. Wang *et al.*, UDP-glucose accelerates SNAI1 mRNA decay and impairs lung cancer metastasis. *Nature* **571**, 127–131 (2019).
46. H. Li, R. Durbin, Fast and accurate short read alignment with Burrows-Wheeler transform. *Bioinformatics* **25**, 1754–1760 (2009).
47. G. G. Faust, I. M. Hall, SAMBLASTER: Fast duplicate marking and structural variant read extraction. *Bioinformatics* **30**, 2503–2505 (2014).
48. J. Gao *et al.*, Identification of 113 new histone marks by CHiMA, a tailored database search strategy. *Sci. Adv.* **9**, eadf1416 (2023).
49. J. Gao *et al.*, CIMAGE2.0: An expanded tool for quantitative analysis of activity-based protein profiling (ABPP) data. *J. Proteome Res.* **20**, 4893–4900 (2021).
50. Y. Chen, S. W. Kwon, S. C. Kim, Y. Zhao, Integrated approach for manual evaluation of peptides identified by searching protein sequence databases with tandem mass spectra. *J. Proteome Res.* **4**, 998–1005 (2005).
51. J. Gao *et al.*, Data from "Characterization of three lactylation isomers lactylation KL-la, KD-la and Kce in hypoxia." iProX. https://www.iprox.cn//page/subproject.html?id=IPX0006076002. Deposited 14 March 2023.

Downloaded from https://www.pnas.org by Univ Joseph Fourier/INPG on October 9, 2026 from IP address 129.88.25.232.